Absolute measurement of lattice parameter in single crystals and epitaxic layers on a double-crystal X-ray diffractometer

M. Fatemi

Electronics Science and Technology Division, Naval Research Laboratory, Washington, DC 20375, USA. Correspondence e-mail: fatemi@estd.nrl.navy.mil

Details of the recently developed 'zone technique' for the absolute measurement of lattice parameter and strain in single-crystal solids and thin films are presented. The method is based on measuring X-ray rocking curves from a few equatorial planes within a suitable zone and correcting their peak positions at once with a single zero offset. In contrast to the comparative method, which usually requires use of two opposite azimuthal directions, those in the zone technique can often be completed in only one azimuthal setting. A typical strained layer in the cubic system can be fully and rapidly characterized with only three rocking curves. The technique is suitable for routine applications under typical laboratory conditions, and for high-precision measurements of nearly perfect crystals in a controlled environment, with a potential parts in 10 million accuracy. This degree of accuracy is a direct consequence of the zero offset correction procedure, which effectively cancels a large portion of the misalignment errors in the diffractometer. The use of the $(n, -n)$ geometry substantially reduces the errors of eccentricity compared to the Bond technique, and its stronger reflections enable the measurement of small samples about 0.05 mm in length with relative ease. The technique is illustrated with examples, and its extension to the triple-axis (ω–2θ) instruments is discussed.

1. Introduction

1.1. Background

The need for accurate determination of unit-cell dimensions and strains in thin films and epitaxic layers has increased pronouncedly in recent years. The impetus for this information is twofold. From a fundamental standpoint, a thorough knowledge of these parameters helps to understand better the nature of atomic bonds in solids. From a technological standpoint, the information is important in the fabrication of electronic devices and materials where interrelated parameters such as strain and bandgap must be stringently controlled. It is desirable, therefore, to have at hand a simple, rapid and readily available laboratory method for the routine determination of absolute lattice parameters. The term 'absolute' implies that the measurements are performed in a controlled environment, by relying exclusively on well known external parameters, such as standard X-ray wavelengths for use in Bragg's law.

One such technique, henceforth referred to as the 'zone technique', was recently introduced by the author (Fatemi, 2002). The method enables the simultaneous and rapid determination of several exact Bragg angles in a given zone. It resolves the well known difficulty with the zero setting in the double-crystal diffractometer by providing a single zero-offset correction for all the measured angles at once. Its simplicity, along with an accuracy of 5–6 significant figures under typical laboratory conditions, was demonstrated in the original paper for a few electronic materials. Its ideal detection limit of better than 2 parts in 10^7, however, makes it equally useful for high-resolution measurements in critical applications. This accuracy, as shown below, is a direct consequence of the zero-offset correction procedure. The zone method contrasts several previously published high-resolution procedures that involve either specialized instrumentation (Hart, 1969) or are hard to extend to different materials or to environments other than synchrotron sources (Zhang et al., 2003).

The main objective of this work is to demonstrate the method's high accuracy and to illustrate further its versatility and speed with examples. Calculations of strain and composition are described in detail, taking into account the dynamical effects of refraction and proximity. The critical factors in instrumental alignment and their effects on measurements are examined. The extension of the method to triple-axis geometries is also discussed

1.2. Historical notes

In a recent work, Gałdecka (1999) gave a detailed review of X-ray diffraction techniques for lattice-parameter measure-

ments in single crystals. Probably the most familiar among these is the Bond method (Bond, 1960), introduced more than four decades ago. Originally introduced on a simple diffractometer with a pinhole collimator, it was based on a clever concept to eliminate the effects of misalignment as well as the unknown zero offset. The need for non-dispersive measurements at higher angles later made it necessary to perform some of the measurements on a double-crystal diffractometer. Fig. 1 shows the concept, using the double-crystal configurations known as 'parallel' $(n, -n)$ and 'anti-parallel' $(n, +n)$. The Bragg angle θ_B is obtained from the angular separation $\pi - 2\theta_B$ between the settings at the two diffraction peaks.

Six years after the introduction of the Bond method, two nearly simultaneous events highlighted the significance and the limitations of that method. Baker *et al.* (1966) introduced a computerized procedure for the Bond technique on a double-crystal diffractometer, and Kikuta *et al.* (1966) documented the first application of the 'comparative' double-crystal technique for epitaxially grown semiconducting layers. Despite its difficulty at the time with thin films, however, the Bond method remained as the 'umpire' technique for reference materials such as high-purity Si.

Similar to the practice in powder diffractometry, the comparative method assumed prior knowledge of the substrate lattice parameter as an 'internal standard'. The method was adopted on the premise that bulk substrates should maintain their characteristic properties throughout the various processing stages. Hence, the two methods together provided an 'acceptable' means of characterizing thin strained layers. In principle, the Bond method would provide the data for the substrate and the comparative method would extrapolate this information to the unknown layer.

### 1.3. Comparison of the Bond, the comparative and the zone techniques

The measurement of thin films and epitaxic layers with the Bond method on a double-crystal diffractometer required very high incident intensities. However, enlarging the beam size for higher intensity only worsened the effects of surface non-uniformity and warping. The asymmetric reflections needed for strain were also difficult to handle with the Bond technique, since they are always measured at unequal diffraction angles where, unlike the symmetric case, the errors of misalignment would not be cancelled out. High-resolution multiple-crystal beam conditioners (Bartels, 1983) with higher-efficiency X-ray sources were later used to increase the resolution. Higher intensities were also sought with the use of rotating-anode X-ray generators and X-ray mirrors. The resolution achievable with X-ray mirrors is somewhat limited, so that extremely high precision diffractometry is still performed without the mirrors. Routine measurements of lattice parameters in thin films by the Bond technique were initially considered either impractical or cumbersome.

In the comparative method, the uncertainties in the reference-layer lattice parameters and strain pose their own problems. While lattice-parameter variations in the substrate

have often been considered negligible in the measurement of strain, novel multilayer structures demand more exact control of this parameter. For example, in wafer bonding applications, the reference layer is generally too thin to be considered as 'fully relaxed'. Occasionally also the atomic registry between the bonded layer and the compliant substrate is less than ideal, so that the effects of rotational strains must be taken into account. The comparative technique by itself cannot address these questions satisfactorily.

The zone method circumvents many of these difficulties. For example, while the Bond technique involves two measurements for each diffraction angle, the zone method uses only one measurement in the customary 'rocking-curve' mode, which corresponds to the double-crystal $(n, -n)$ or 'parallel' geometry. The notation $(n, -n)$ was originally connected with the fact that both crystals in the diffractometer are set for the same reflection order, whereas in general any two orders such as n and m could be used (see §4.1). The term 'parallel' refers to the fact that the diffracting planes of the two crystals may at some point during the scan become nearly parallel. The term 'anti-parallel' was then adopted to convey the other configuration of the two crystals for the same reflection.

The rocking-curve mode is not only helpful in determining the peak positions more accurately, but it also reduces substantially the errors of eccentricity, which can be quite serious for bent crystals. The use of a bright point source and a single-tube collimator on the double-crystal diffractometer ahead of the first crystal permits rocking-curve measurements from extremely small areas only a few tens of μm wide. Moreover, while typical measurements in the comparative technique require two opposite azimuthal orientations, those
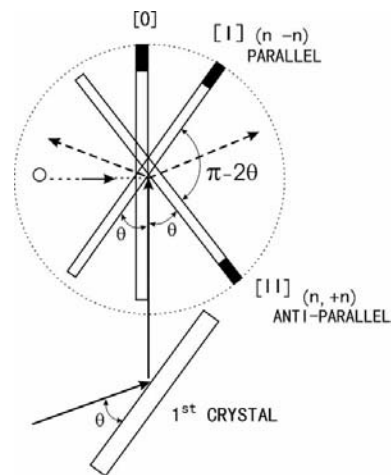
Figure 1
The Bond technique on a double-crystal diffractometer. The incident beam originating from the first crystal (beam conditioner) arrives at the sample surface at point *O*. Position [I] corresponds to the orientation of the wafer in the parallel geometry. A symmetric reflection such as 004 is recorded at the crystal angle $\omega \simeq \theta_B$ with the detector at $2\theta_B$. A second symmetric reflection is recorded in position [II], corresponding to the anti-parallel geometry at the crystal angle $\omega \simeq \pi - \theta_B$. Dashed arrows to the right and left denote the diffracted beams in positions [I] and [II], respectively. Once corrected for refraction, the difference between the two ω settings is $\pi - 2\theta_B$.

in the zone technique can often be completed at a single azimuthal setting. The zone method is particularly fast for most cubic crystals, which can often be characterized with only two or three reflections, depending on the degree of symmetry in the strain.

2. Characteristic features of the zone technique

2.1. The basic principle

The striking feature of the zone technique is its simplicity: it provides a means of measuring several absolute Bragg angles sequentially without the need to realign each plane separately for the tilt or azimuth. The general procedure is as follows: (i) orient any suitable crystallographic zone containing two or more strongly diffracting planes into the equatorial direction (all single-crystal materials have at least one such zone); (ii) record the corresponding rocking-curve peak positions; (iii) adjust the peak positions for refraction and proximity effects, if any; (iv) calculate the common zero offset for all the peaks to obtain the 'exact' Bragg angles and hence their related d spacings; (v) finally, use the latter in appropriate equations to obtain the sought unit-cell dimensions. The only instrumental requirement is a well aligned diffractometer having a high-resolution (0.0001°) θ circle, reproducible within $\pm$ 0.0001°. The same high resolution, however, is not needed for the detector angle, except that its window must be vertically restricted, subject to the caveats discussed later.

The procedure described in the following sections is aimed at the most efficient way to obtain precise lattice parameters in a laboratory environment for quick turn-around applications. For these applications, five or six significant figures will be more than sufficient. As can be readily seen, it is convenient in most cases to use a pair of asymmetric reflections together with a single symmetric reflection to completely characterize a layer. This is not a fast and rigid rule, as any set of three independent measurements can be used instead, although the computational process would become more involved. For improved accuracy, however, the lower diffraction angles should be avoided as much as possible (see below). Aside from the fact that the shallower angles lead to larger areas viewed by the beam, the step resolution in the θ circle (± 0.0001) can be the limiting factor in determining the final accuracy. For example, with θ_B of about 35°, $\Delta\theta \simeq 0.0002°$ implies a fractional error ($\Delta d/d$) of about 6.5×10^{-6} in the lattice parameter, whereas, with θ_B near 70°, the error is reduced to 1.1×10^{-6}. Of course, since nearly all measurement angles are accessible in this method, the final accuracy depends almost entirely on the extent of effort and available time.

Fig. 2 shows a sketch of an equatorial zone with several member planes perpendicular to the diffractometer table. The angles among these planes are connected by simple linear relationships. Thus, if the X-ray beam is set for diffraction from plane 1, the ω setting for plane 2 is found from a linear combination of their corresponding Bragg angles and their interplanar angle β_{12}. It follows that a 'reading error' in the

angular setting for any plane would apply equally to all other planes in the zone. This obvious and trivial property of the equatorial planes is the basis of the zone technique.

2.2. The basic formulation

Consider two equatorial planes with interplanar spacings d_1 and d_2, respectively, where d_1 refers to the symmetric (surface plane) reflection and d_2 to a pair of asymmetric planes with equal and opposite angles $\pm \beta_{12}$ with respect to the symmetric plane. Following the customary rocking-curve procedures, the crystal is brought into the beam at the approximate zero setting, the so-called 'starting position'. Rocking-curve peaks are then found at three angles ω_1 (symmetric reflection), ω_{2sh} (shallow or glancing incidence) and ω_{2stp} (steep or glancing exit), respectively. Clearly all recorded angles will then be offset by an initially unknown value ε. We write

$$\lambda = 2d_1 \sin(\theta_1 + \varepsilon), \tag{1a}$$

$$\lambda = 2d_2 \sin(\theta_2 + \varepsilon). \tag{1b}$$

In these expressions, the Bragg angle for the symmetric plane is given by $\theta_{B1} = \theta_1 + \varepsilon = \omega_1 + \varepsilon - \Delta\omega_{sym}$, where ω_1 is roughly the angle between the crystal surface and the incident ray at the peak of the rocking curve and $-\Delta\omega_{sym}$ is the corresponding refraction correction. Similarly, the Bragg angle for the asymmetric plane is $\theta_{B2} = \theta_2 + \varepsilon$, where $\theta_2 = \omega_{2sh} + \beta_{12} - \Delta\omega_{sh}$ or, equally, $\theta_2 = \omega_{2stp} - \beta_{12} - \Delta\omega_{stp}$.

As seen later, the refraction corrections are small enough to be ignored in the first approximation in order to simplify the calculations. Thus, equation (1b) could be written in one of two equivalent forms:
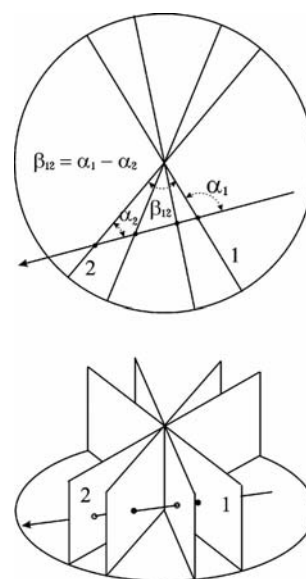
Figure 2
The principle of the zone technique. A crystallographic zone is oriented in the equatorial direction. The planes belonging to this zone are parallel to the rotation axis and perpendicular to the diffractometer table. The angle β_{12} between any two planes, *e.g.* 1 and 2, is equal to the difference between the angles α_1 and α_2 between the incident beam and the two planes.

$$\lambda = 2d_2 \sin(\omega_{2sh} + \beta_{12} + \varepsilon) \qquad (1c)$$

$$\lambda = 2d_2 \sin(\omega_{2stp} - \beta_{12} + \varepsilon). \qquad (1d)$$

Each measured ω would then be adjusted by its own refraction correction (§2.3.1) following the calculation of ε (note that the precise argument in these expressions would have the form $\omega_{2sh} + \beta_{12} + \varepsilon - \Delta\omega_{sh}$ *etc.*). To solve equations (1a) and (1b), we need one more independent relationship, *e.g.* the one connecting the measured interplanar angle corresponding to d_1 and d_2. In the particular case of crystals with cubic and tetragonal symmetry, one can show that, if $d_2 < d_1$,

$$d_2/d_1 \equiv k = \cos\beta_{12}, \qquad (2)$$

Relations quite similar to equation (2) can be found for other structures, such as the hexagonal, at various orientations (see §3.3.3 below).

If the zero offset ε is small compared to θ_1 and θ_2, then

$$\varepsilon = \frac{k \sin\theta_2 - \sin\theta_1}{\cos\theta_1 - k\cos\theta_2}. \qquad (3)$$

For materials such as (100) Si, a 'symmetric' rocking curve, 004, and a pair of asymmetric ones, *e.g.* 224, will suffice. The asymmetric peak positions yield two important numbers. One is their difference $\omega_{stp} - \omega_{shl} = 2\beta_{12}$, which is independent of the zero offset, except that each ω must be separately corrected in advance. The other is the sum $\omega_{stp} + \omega_{shl} = 2(\theta_{B2} + \varepsilon)$, where again each ω is to be corrected for refraction. This will be illustrated later in the examples. These two quantities and the symmetric peak $\theta_1 + \varepsilon$ supply all the needed data to characterize the layer with the aid of the linear elasticity theory. The relationships just examined remain valid for curved diffracting planes, provided that the diffractometer is aligned properly to eliminate the eccentricity effects as described later.

The zone method becomes particularly elegant for *bulk* crystals having two or more allowed orders of symmetric reflection. All cubic III–V compounds, hexagonal structures such as III-N and SiC, as well as (111)-oriented Si and Ge, are in this group. For these materials, the d spacings of the symmetric (basal plane) reflections are related to each other by integer ratios, *i.e.* $k = m/n$, where m and n are two different reflection orders. For cubic crystals in this group, the asymmetric reflections are not needed, as they are identified with only a single lattice parameter. However, the procedure applies also to the *fully* strained layers, such as GaAlAs layers on GaAs, where the relationship between the in-plane and perpendicular lattice parameters is established from linear elasticity. In the hexagonal structure, by contrast, the 'a' and 'c' lattice parameters are related through a pre-determined c/a ratio. The same procedures can also be used for crystals without the fourfold or mirror symmetry, *e.g.* strained 3*C*-SiC on 4*H*-SiC, with minor additional considerations (Fatemi *et al.*, 2004).

2.3. Dynamical effects

2.3.1. Refraction 'corrections'. Refraction, *i.e.* the dynamical deflection of the X-ray beam in the interior of the crystal towards the surface, is often safely ignored in routine applications such as rocking-curve simulation and line-broadening studies. However, it is an essential component of any absolute method, including Bond's, for obtaining correct results. The term 'correction' is a misnomer, as the effect is not an error but merely a well defined adjustment to otherwise accurately measured crystal angles for use with Bragg's law. The adjustments have well known values and are universally invariant for any given material and wavelength. Hence, they can be placed in a 'look-up' table and referred to as needed. The atomic scattering factors used in their calculation are available from a number of sources (Cullity, 1987; Maslen *et al.*, 1999; Rupp,[1] World Wide Web). Furthermore, they are an inherent component of any correctly composed dynamical simulation algorithm, where they can be recorded directly as the displacement between the diffraction peak and the 'zero' coordinate of the simulation plot.

Each measured angle ω must first be corrected for refraction by subtracting from it the quantity $\Delta\omega$ defined by (James, 1963)

$$\omega_B = \omega_m - \Delta\omega \qquad (4)$$

$$\Delta\omega = \delta_n(\tan\theta_B + \cot\omega_B), \qquad (5)$$

where ω_B is the offset-corrected incidence angle at the Bragg condition, ω_m is the measured angle and θ_B is the Bragg angle. The deviation δ_n from unity of the index of refraction is defined by

$$\delta_n \equiv 1 - n = \frac{\lambda^2 e^2}{2\pi V mc^2} F_{hkl} = 1.06 \times 10^{-5} \frac{F_{hkl}}{V}. \qquad (6)$$

In this expression, the unit-cell volume V, the X-ray wavelength λ (here Cu $K\alpha_1$ radiation) and the classical electron radius e^2/mc^2 are in Å-based units, and F_{hkl} is the unit-cell structure factor for the particular reflection. Note that in order to use equations (1a) and (1b) the angle ω_B must first be converted to a 'θ' angle as remarked earlier.

It is instructive to examine equation (5) in some detail. The expression connects an unknown quantity $\Delta\omega$ to two variables ω_B and θ_B, both of which depend on the same unknown $\Delta\omega$: the first through equation (4), the second through ω_B after adjusting for the vicinality of the diffracting planes (see below). The explicit expression for $\Delta\omega$ is therefore

$$\Delta\omega = \delta_n[\tan(\omega_m - \Delta\omega \pm \alpha_{12}) + \cot(\omega_m - \Delta\omega)], \qquad (7)$$

where α_{12} is a general term that represents any combination of the interplanar and vicinal angles. As with β_{12}, it is either added to or subtracted from ω_m. Although this expression appears rather formidable, its exact solution is not often necessary, since the effect of $\Delta\omega$ on the right-hand side is negligible compared to other terms. For practical purposes, therefore, one may initially replace the angle ω_B with ω_m, and thus ignore $\Delta\omega$ terms on the right.

The effect of the vicinal angle on refraction, however, can be significant, especially in the glancing entrance mode.

---

[1] Atomic scattering factors at http://www-structure.llnl.gov/xray/comp/scatfac.htm [site maintained by Bernhard Rupp (br@llnl.gov)].

Assume, for example, that the 224 reflection is measured from a 3°-miscut Si (100) wafer, such that the equivalent ω_{sh} is about 5.75°, rather than the 'on-axis' value of about 8.75°. The second term in equation (7), namely $\cot(\omega_B)$, would then change from ≈ 6.5 to 10, increasing the value of $\Delta\omega$ in turn by $\approx 50\%$. To prevent very large errors in the refraction term, therefore, one must avoid low-angle reflections as much as possible. As the adjustments are mostly in the arc s regime, their uncertainty should not exceed 5–10%. In the present case, a miscut angle of 0.5° would change the cotangent term from 6.5 to 6.9, or ~+6%. If a large miscut is suspected, it should be determined reasonably well before attempting high-precision measurements. The methods available for this purpose range from the customary Laue back-reflection technique, accurate within ±0.25°, to very high precision using a combination of visible laser optics and X-rays, accurate to about 1 arc s (Fatemi, 1990).

It should be noted that the numerical hand calculation of the refraction correction must give nearly identical results to those available on a properly written dynamical simulation for the specific crystal being examined.

2.3.2. The proximity effect. In a system containing two coherent structures with nearly similar d spacings, the two diffraction peaks move towards each other from the position predicted by Bragg's law. Thus, to use Bragg's law with the zone technique, the measured angles must first be corrected for the proximity effect. This dynamical phenomenon has been established both experimentally and theoretically (Fewster & Curling, 1987; Wie, 1989). As it is most noticeable for thinner layers, it has been loosely referred to as the 'thin-film effect', although layers of any thickness with a small angular separation (few hundred arc s) between them show the same effect. The most reliable values are found through the dynamical

Figure 3
Schematic representation of the critical parameters of misalignment on a double-crystal diffractometer: the incident X-ray beam vertical slant γ and the tilts δ_1 and δ_2 corresponding to the beam conditioner and the second crystal, respectively. The unit vectors $\mathbf{e}_1$ and $\mathbf{e}_2$ are parallel to the diffractometer table. The detector window is fitted with a horizontal slit, whose vertical opening is nearly the same size as the X-ray focal spot. The combined effect of the three misalignment parameters determines the location of the incident beam as it arrives at the detector.

simulation of rocking curves for layers with assumed thickness and composition similar to those being measured.

3. Alignment considerations

3.1. Instrumental requirements

Accurate measurement of crystal angles in the zone technique consists of two steps; one, the mechanical alignment of the instrument, the other, the alignment of an equatorial zone. The mechanical alignment requires not only that the rotation, azimuth, and tilt axes be mutually orthogonal, but also that the incident beam be centered with these axes at the same point on the sample surface. Most commercial diffractometers are factory aligned and need only minor adjustments at the installation site. These adjustments consist of aligning the X-ray source with the beam conditioner and the slits following it, which together help orient the incident beam in a horizontal direction parallel to the diffractometer table. Specific procedures can also be devised for 'custom-made' instruments. Modern optical tools, such as self-leveling lasers, null-setting LEDs and high-precision rotation stages can be used to streamline and simplify the process. Detailed articles by Thomsen (1973) and Fewster (1985) provide further guidance.
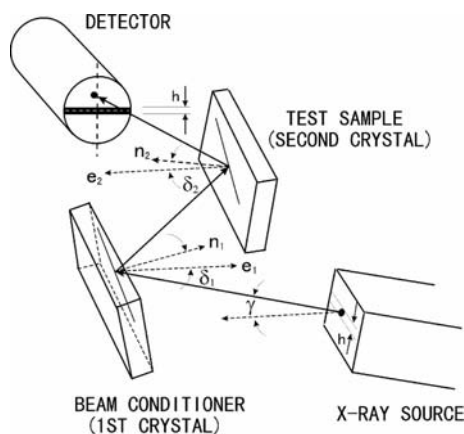
The detector-window configuration is important. In the zone technique, it is fitted with a narrow horizontal slit to confine the X-ray beam to the central plane. Its vertical opening should be no wider than the height of the X-ray source, while its lateral dimension can be as wide as desired. This particular configuration helps eliminate nearly all misalignment errors in the diffractometer. These result mostly from vertical deviations in various segments of the beam from the source to the detector (see also the discussion on the triple-axis diffractometer, §4 below). Fig. 3 shows the critical factors, namely, the slant γ of the incident beam as it emerges from the X-ray source and the vertical tilts δ_1 and δ_2 in the first and second crystals, respectively.

3.2. Sample alignment in the zone technique

The expression 'sample alignment' in this work means that a crystallographic zone is made equatorial so that all its diffracting planes can be measured without readjusting the sample tilt or azimuth between the measurements.

The alignment procedure is nearly the same in diffractometers with different sample holders. Most modern diffractometers use an Eulerian cradle, in which the tilt adjustment arm (χ) is the 'primary' mechanism that carries the remaining movements of azimuth (ϕ) and translation. With this holder, the crystal can be brought rapidly into any desired orientation from a known starting point. However, the vicinality in the sample, irregularities in the mounting surface and mechanical instabilities in the diffractometer all affect the starting angle. Hence, a few iterations may be needed to reach the optimum 'equatorial' setting (following section).

Another type of sample holder is the 'Cartesian' holder, designed by the author in a modified double-crystal instrument (Fatemi, 1989). Here, the primary mechanism is the

azimuth, which supports the movements of tilt and translation. This arrangement helps to align rapidly the tilt vector of the symmetric planes with the azimuth axis. The asymmetric planes can therefore be made equatorial by a simple rotation of the sample about the azimuth axis. The Cartesian holder is

Figure 4
Exaggerated schematic representation of the sequence of operations needed to bring a cubic crystal from an arbitrary orientation into a zone-aligned state. The sample is a (100)-cut Si wafer, whose 110 zone is inclined relative to the diffractometer table (*xy* plane). The X-ray beam, parallel to the *xy* plane, arrives at the sample from the right. (*a*) Initial orientation. The symmetric [001] and the asymmetric [224] plane normals point to two arbitrary directions in space, with the (001) planes tilted 'up', the (224) planes tilted 'down'. The [001] axis is made horizontal with the 004 rocking curve, using only the tilt mechanism (angle δ). The detector is placed at the approximate $2\theta_B$ for Cu $K\alpha_1$ radiation, 69°, and the crystal angle (ω) near 34.56°. Once the peak is found, its intensity and sharpness (FWHM) are optimized using *only* the tilt (χ). (*b*) Intermediate orientation. The asymmetric planes 224 or 2̄24 are aligned sequentially, with the detector placed at $2\theta \simeq 88°$ (Cu $K\alpha_1$ radiation), and the crystal angle ω to the position corresponding to either the shallow reflection $\omega_{sh} \simeq 8.75°$ or the steep $\omega_{stp} \simeq 79.25°$. The diffraction peaks are optimized by varying the azimuth (ϕ) alone. (*c*) The wafer in the final zone-aligned orientation. All planes in the (110) zone can now be measured without any further refinement in their tilt or azimuth.

more efficient for the zone technique and for the measurement of vicinal angles, while the Eulerian cradle is better suited for complex movements such as those connected with reciprocal-space mapping.

3.2.1. Alignment details. Fig. 4 is a schematic representation of the procedure using the Cartesian holder for aligning the (110) zone in an Si (100) wafer, as described previously (Fatemi, 2002). It consists of alternately adjusting the tilt and azimuth settings for the symmetric and asymmetric planes within the zone. Similarly, hexagonal structures, *e.g.* 4H-SiC, sapphire (Al$_2$O$_3$), GaN *etc.*, can be aligned, each using their own appropriate asymmetric planes.

After sample alignment, all diffracting planes within the zone are correctly oriented, and can be measured by the familiar rocking-curve technique.

3.3. Measurement of homogeneous strain with the zone technique

An epitaxic layer deposited on a substrate is in general under some form of strain. For example, an SiGe layer with $x_{Ge} = 0.2$ and a thickness of 0.25 µm is partially relaxed, whereas a GaAlAs layer remains fully strained for up to several µm thickness. In the latter case, a single measurement of the perpendicular lattice parameter would suffice, since by definition the in-plane lattice parameter is fully matched to the substrate, which is measured independently by the same method also.

The general application of the zone technique begins with the calculation of the offset angle according to equations (1)–(3). Next, the unit-cell parameters in the epitaxic layer are calculated (Fatemi, 2002). Since these dimensions often correspond to a strained layer, the appropriate crystal model, *e.g.* tetragonal structure for strained cubic crystals, is used to derive the bulk lattice parameters with the aid of the linear elasticity theory, and hence the composition of the layer using Vegard's law. In most cases, it is also possible to derive a number for the interlayer tilt as the (vector) difference between the zero offsets for the substrate and the epilayer.

3.3.1. Cubic unit cell under tetragonal distortion: SiGe layer on Si. If the perpendicular and in-plane lattice parameters are denoted as $a_\perp$ and $a_\parallel$, the relaxed (bulk) lattice parameter a_r in the SiGe layer is found from
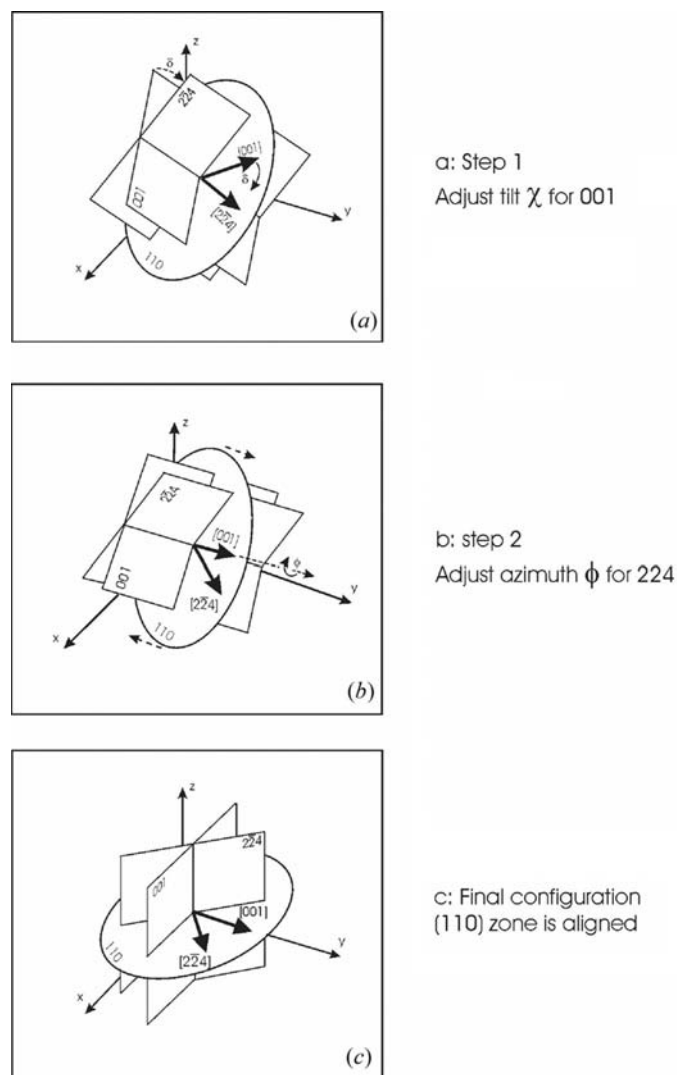
$$a_\perp - a_r = -2\frac{c_{12}}{c_{11}}(a_\parallel - a_r), \qquad (8)$$

assuming tetragonal distortion (Fatemi & Stahlbush, 1991). Here, c_{12} and c_{11} are the elastic constants for the alloy under the assumed composition. The epilayer strain s is defined as the ratio of the change in the in-plane lattice parameter $a_\parallel$ to the maximum change available to it:

$$s = \frac{a_\parallel - a_{Si}}{a_r - a_{Si}}, \qquad (9)$$

where a_{Si} and a_r denote the bulk lattice parameters of Si and SiGe, respectively.

The Ge composition x_{Ge} is found by applying Vegard's law (Dismukes *et al.*, 1964; Fatemi, 1996):

$$x_{Ge} = \frac{a_r - a_{Si}}{a_{Ge} - a_{Si}}. \tag{10}$$

If the composition calculated from this expression is different from the one initially assumed, one could perform iterations of (8) and (10) until consistent results are obtained.

3.3.2. Strain measurement in the hexagonal system. In the hexagonal system, when the epilayer and the substrate have similar symmetries, the strain in the layer can be obtained from definition (9). This definition, however, cannot be applied to mixed systems where the two layers have different orientations, as in the case of a 'c-plane' GaAlN layer deposited on an a-plane sapphire substrate (Fig. 5), since there is no alignment between equivalent interatomic dimensions for comparison.

One possible, albeit indirect and arbitrary, way to define the strain in such systems is through the change in the c/a ratio (or somewhat more logically, its inverse, a/c) for a given composition in the strained layer compared to the bulk (unstrained) material. This implies of course that predetermined values for the bulk material are indeed available. As of this writing, there is still some ambiguity regarding standard values for most hexagonal structures. Presently, the c/a values for GaN and AlN are 1.6258 and 1.6002, respectively, based on $a(\text{GaN}) = 3.1893$, $c(\text{GaN}) = 5.1851$, $a(\text{AlN}) = 3.1130$ and $c(\text{AlN}) = 4.9816$ Å. If we also assume Vegard's law to hold strictly, the bulk (unstrained) lattice parameters for a GaAlN layer containing 30% AlN become: $a(\text{GaAlN}) = 3.1664$, $c(\text{GaAlN}) = 5.1241$ Å, leading to $c/a = 1.6182$. The observed ratio for a strained layer would be different depending on the type and the crystallographic orientation of the substrate.

To conform to the usual formulation in the cubic system, we use the inverse of the c/a ratio, namely a/c, since the 'in-plane' reference lattice parameter in the basal plane growth is the a

Figure 5
Stereographic projection of a basal-plane (0001) GaN, or similar material, grown on a-plane (11$\bar{2}$0) sapphire (Al_2O_3) substrate, showing reflecting planes used in the measurements. The 'main flat' marks the substrate c axis, i.e. the zone (0001), oriented in the equatorial direction. Planes of type (11.3) and (22.3) from the substrate and (10.5) from the epilayer are aligned, and can thus be measured simultaneously for rocking curves. Solid circles, marked by suffix s, refer to the substrate; hollow circles, suffix e, refer to the GaN layer. Note the slight misalignment between the projections of the ($\bar{1}$1.9) s and (21.0) e etc. planes.

dimension of the unit cell. The strain s_{Hex} could then be defined as

$$s_{Hex} = \frac{\kappa_m - \kappa_r}{\kappa_m - \kappa_s}, \tag{11}$$

where $\kappa \equiv a/c$, and the subscripts m, r and s denote, respectively, the measured and relaxed (bulk) values of a/c in the epilayer and its corresponding value in the substrate.

The epilayer alloy composition in the hexagonal system is derived in a manner similar to the cubic system. In the present case,

$$x_{Al} = \frac{ac(1 + \alpha) - \alpha c a_1 - a c_1}{\alpha c(a_2 - a_1) + a(c_2 - c_1)}, \tag{12}$$

where the subscripts 1 and 2 refer to the known or predetermined lattice parameters of the constituents GaN and AlN, respectively, and α is defined as

$$\alpha = 2\frac{c_{12}}{c_{11}}. \tag{13}$$
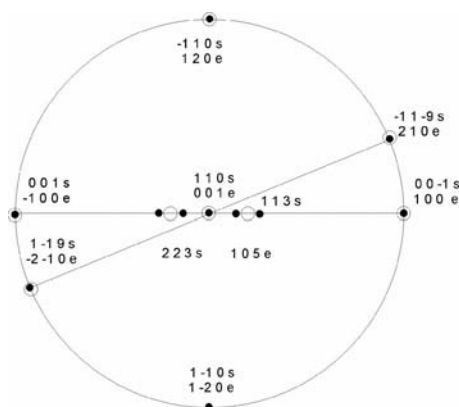
Equation (12) is derived from the general relationship

$$\frac{c - c_0}{c_0} = -\alpha\left(\frac{a - a_0}{a_0}\right), \tag{14}$$

where the parameters a and c denote the *measured* lattice parameters in the layer and the subscript 0 refers to the corresponding bulk (relaxed) parameters as determined from linear elasticity theory.

The expressions for interplanar angles and the d spacings in the hexagonal system (Cullity, 1987) provide ancillary information for solving equations (1a) and (1b):

$$\frac{1}{d_{hkl}^2} = \frac{4}{3}\left(\frac{h^2 + hk + k^2}{a^2}\right) + \frac{l^2}{c^2} \tag{15}$$

$$\cos\phi = \frac{h_1 h_2 + k_1 k_2 + \frac{1}{2}(h_1 k_2 + k_1 h_2) + \frac{3a^2}{4c^2}l_1 l_2}{\left[\left(h_1^2 + k_1^2 + h_1 k_1 + \frac{3a^2}{4c^2}l_1^2\right)\left(h_2^2 + k_2^2 + h_2 k_2 + \frac{3a^2}{4c^2}l_2^2\right)\right]^{1/2}}. \tag{16}$$

3.3.3. A numerical example. Consider the growth of a GaN or similar layer on an a-plane sapphire wafer, with nominal parameters $a_0 = 4.7589$, $c_0 = 12.991$ Å (Lee & Lagerloff, 1985). The orientation of the epilayer relative to the substrate is shown in the combined stereographic projection in Fig. 5. We see that all the needed measurements can be obtained at a single azimuth by orienting the wafer such that the substrate's c zone (0001) is equatorial. In this case, each layer is characterized with only three rocking curves.

For the GaN epilayer, the symmetric 0004 and the asymmetric reflections 10$\bar{1}$5 and $\bar{1}$015 provide strong, relatively sharp, rocking curves. The sapphire substrate is measured with the symmetric 22$\bar{4}$0 (a-plane reflection) combined with a pair of asymmetric reflections from either (22$\bar{4}$3)-type planes, 15.35° away from the a axis, or (22$\bar{4}$6), i.e. second-order (11$\bar{2}$3)-type planes, at 28.75° away. The (22.3) planes have a lower Bragg angle but a higher glancing incidence angle $\omega_{shl} \simeq$ 26.5° (Cu $K\alpha_1$ radiation), compared to the (22.6) planes, $\omega_{shl} \simeq$

Table 1
X-ray rocking-peak positions for an Mg-doped GaN layer grown on an *a*-plane (11.0) sapphire.

All measurements were made under controlled room temperature of 294.6 K in one azimuthal direction with both GaN and sapphire zones aligned.

Reflection	ω (peak) (°) (measured)	FWHM (° / arc s)	ω (peak) (°) (corrected)	d spacing lattice parameter (Å)
Sapphire (22.0) symmetric	40.1885	0.0050 / 18	40.3561	$d_{220} = 1.18956$ $a = 4.75824$
Sapphire (22.3) shallow	26.6555	0.0057 / 20.5	26.8231	$d_{223} = 0.912836$ $c = 12.98977$
Sapphire (22.3) steep	57.3796	0.0053 / 19.1	57.5472	
GaN 0004 symmetric	36.2862	0.1422 / 512	36.4584	$d_{004} = 1.296249$ $c = 5.18499$
GaN (10.5) shallow	31.7476	0.1405 / 506	31.9137	$d_{105} = 0.970722$ $a = 3.18648$
GaN (10.5) steep	72.9382	0.1757 / 632	73.1109	

18.6°. As noted in §2.3.1 above and also later below, the higher glancing angles are generally preferred since they lead to less uncertainty in the refraction correction.

For the planes of type (22.3) in the *a*-plane (11$\bar{2}$0) Al$_2$O$_3$:

$$\cos \angle(22.3, 11\bar{2}0) = \frac{2}{(4 + 9a^2/4c^2)^{1/2}}, \qquad (17)$$

$$1/d_{223}^2 = 16/a^2 + 9/c^2 \qquad (18)$$

and

$$1/d_{22.0}^2 = 16/a^2. \qquad (19)$$

From (16)–(18), we can also derive the condition

$$d_2/d_1 \equiv k = \cos \beta_{12}, \qquad (20)$$

where $d_2 = d(22\bar{4}3)$ and $d_1 = d(22\bar{4}0)$, and β_{12} is obtained from the measurements.

Similarly for $(h0\bar{h}l)$-type planes in the *c*-plane (0001) GaN, we obtain from equations (15) and (16):

$$\cos \beta \equiv \cos \angle(10,\bar{1},l, 0001) = \frac{[\frac{3}{4}(a^2/c^2)]^{1/2}}{[1 + \frac{3}{4}(a^2/c^2)]^{1/2}}, \qquad (21)$$

$$1/d_{10.5} = 4/3a^2 + 25/c^2, \qquad (22)$$
$$1/d_{0004}^2 = 16/c^2 \qquad (23)$$

and, thus,

$$d_2/d_1 \equiv k = \tfrac{4}{5} \cos \beta_{12}, \qquad (24)$$

where $d_2 = d(10\bar{1}5)$ and $d_1 = d(0004)$. Note the slight difference in the multiplier on the right-hand sides in equations (20) and (24)!

We apply these formulas to a system consisting of a 1.0 µm layer of Mg-doped GaN deposited on an *a*-plane sapphire substrate. To eliminate the effect of variations in the sample surface and warping, a small beam of approximately 0.1 × 0.5 mm in cross section was used, although with care

smaller areas about 0.05 × 0.1 mm have also been measured (Fatemi, to be published). Owing to the beam spread, the area covered is about twice as large, yet well within the acceptable limits. We expect to see different lattice parameters for the Mg-doped GaN compared to the 'undoped' sample. To reduce the uncertainty due to small drifts in peak positions, each measurement is both preceded and followed by the rocking curve from a sharp substrate reflection, in this case the sapphire 22$\bar{4}$0 reflection. This practice is helpful in reducing the measurement errors. For moderate monotonic drifts, it is possible to make an adjustment in the 'unknown' peak position by interpolating between the times corresponding to the reference peaks. The more 'random' variations may indicate mechanical and thermal instabilities that would have to be addressed before collecting the data.

As usual with all high-precision measurements, repetition is essential. We also note that, in order to estimate the peak positions precisely, each rocking curve need only be measured – with suitable counting times – in a range of angles just outside the FWHM.

Table 1 shows the normalized data for the system just described, using the 004 reflection from an Si(100) beam conditioner with Cu $K\alpha_1$ radiation. During several hours of such measurements, only a slight monotonic drift of approximately 2.5 arc s was detected for the reference (22.0) rocking curve, and no two consecutive reference peaks differed by more than 0.3 arc s.

The sapphire and GaN offset angles are each obtained from their own set of peaks. Laue back-reflection patterns show that the 'basal planes' *a* and *c* of sapphire and GaN are nearly aligned, and that the vicinality is negligible. Hence, the approximate 'Bragg' angles of the asymmetric reflections can be used for the refraction correction. Solving equation (3), however, requires independent expressions such as equations (20) and (24) in each case, similar to equation (2) for the cubic crystals.

Calculations begin with refraction corrections. From (5) and (6), we have for sapphire 22.0 reflection

$$\Delta\omega(22.0)_{\text{sym}} = \delta_n(\tan 40.1885 + \cot 40.1885) = 2.028\delta_n$$

and

$$\delta_n \equiv 1.06 \times 10^{-5}(F_{hkl}/V),$$

with $f_{Al} = 6.39$, $f_O = 2.77$, $F_{440} = 21.09$, $V = 0.866ca^2 = 248$ Å^3, leading to $\Delta\omega = 1.828 \times 10^{-6}$ rad $= 1.05 \times 10^{-4\circ}$. Similarly, for $(223)_{\text{shl}}$, $f_{Al} = 6.22$, $f_O = 2.66$, $\Delta\omega(223)_{\text{shl}} = 2.893\delta_n = 1.52 \times 10^{-4\circ}$, and $\Delta\omega_{\text{stp}} = 2.20\delta_n = 1.1 \times 10^{-4\circ}$. We see that all three angles are to be corrected downwards by nearly equal amounts, ~0.0001°. Within the practical limits in these measurements, we may therefore safely ignore this adjustment, since the effect would ultimately be removed by the

Table 2
Calculation of the peak shifts and their difference (residual) error for the pair of 004 and 224 reflections in Si(100).

In the fourth column, all numbers are rounded to the fifth decimal place, corresponding to the practical resolution expected from the rocking curves. Columns 2 to 4 show the results for an assumed misalignment level of $\pm 0.05°$ in each of the three parameters γ, δ_1 and δ_2. The last column shows the final results assuming $\pm 0.02°$ variation in each parameter. In this case, the corrections are small enough to be rounded to the sixth decimal place for use with higher-precision measurements. A large portion of the contribution to the individual θ_c errors is purged by the subtraction process, thus greatly reducing the misalignment effect.

γ, δ_1, δ_2 (°)	θ_{c1}, 004 (°)	θ_{c2}, 224 (°)	Residue $\theta_{c2} - \theta_{c1}$ ('0.05°') (°)	Residue $\theta_{c2} - \theta_{c1}$ ('0.02°') (°)
+0.05. +0.05, +0.05	−0.00002	−0.00003	−0.00001	−0.000001
+0.05, −0.05, +0.05	+0.00003	+0.00001	−0.00002	−0.000003
+0.05, +0.05, −0.05	−0.00001	−0.00001	−0.00000	−0.000001
+0.05, −0.05, −0.05	−0.00020	−0.00025	−0.00005	−0.000001

zero offset correction. The same considerations apply to the GaN layer.

To calculate the lattice parameters, we first find from Table 1 $\beta_{\text{saph}}(22.3, 11.0) \simeq \frac{1}{2}(57.3796 - 26.6555) = 15.3620°$, and $\beta_{\text{GaN}}(10.5, 00.1) \simeq 20.5953°$. From equation (20), $d_2/d_1 = 0.964271$, and hence the zero offset, $\varepsilon_{\text{saph}} = +2.9280 \times 10^{-3}$ rad $= +0.1676°$. Similarly for GaN, $k_{\text{GaN}} = 4/5 \cos \beta = 0.748871$ and $\varepsilon_{\text{GaN}} = +3.006 \times 10^{-3}$ rad $= +0.1722°$. The small discrepancy of 17 arc s between the two zero offsets is still considerably larger than the reading error in the GaN peak positions and may thus be kept in mind as a possible slight interlayer tilt, subject to further tests.

Using the corrected values of the angles shown in Table 1, we find for sapphire: $a = 4.75823$ and $c = 12.98977$ Å. Similarly for the Mg-doped GaN, we find $c = 5.18499$ and $a = 3.18648$ Å. Both groups of results are comparable to the values listed earlier. The c/a ratio for this GaN layer is 1.62718, which differs from the 'accepted' value 1.62578 for the undoped GaN. One could thus in principle calculate the strain based on its modified definition in equation (11), provided also that Vegard's law holds. While outside the scope of the present work, both these facts must first be established.

4. Instrumental alignment and resolution issues

4.1. Analysis of misalignment errors

In the original paper (Fatemi, 2002), it was pointed out that results with accuracies exceeding five significant figures are easily obtained with reasonable instrumental alignment under typical laboratory conditions. To better quantify that statement, we now examine the effects of various misalignment parameters in more detail. We shall see that, although each individual measurement of the diffraction angle may be subject to a large misalignment error, the process of zero-offset calculation eliminates most of these errors, leaving only a much smaller residue as the final error.

In the double-crystal diffractometer, the deviations γ, δ_1 and δ_2 defined in Fig. 3 collectively produce a shift error θ_c in the measured (recorded) crystal angle, given by (Thomsen, 1973)

$$\theta_c = -\frac{\delta_2^2 + \Psi^2}{2} \tan \theta_n + \frac{\Psi \delta_2}{\cos \theta_n}, \quad (25)$$

$$\Psi = \gamma - 2\delta_1 \sin \theta_m. \quad (26)$$

θ_c denotes an algebraic correction to each measured angle. Here θ_m and θ_n are the Bragg angles for the first and second crystals, respectively. We retain the subscripts m and n as used by Thomsen to avoid confusion with the numerals 1 and 2 in equations (1a) and (1b).

The expression for θ_c in equation (25) can easily be analyzed to determine its largest absolute values. The first term is a monotonically decreasing function of δ_2 and Ψ. Hence, the largest negative shift θ_c occurs when the second term is also negative, that is, when Ψ and δ_2 have opposite signs. If $\delta_2 < 0$, then $\Psi > 0$, and the largest Ψ is found for a positive beam slant γ combined with a negative tilt δ_1. Similarly, when $\delta_2 > 0$, $\Psi < 0$, the latter having its largest magnitude at the largest negative γ. Thus, assuming that each of the three parameters can attain values within $\pm 0.05°$ from the ideal (0°) setting, the largest θ_c would then occur either for $\gamma = 0.05°$ and $\delta_1 = \delta_2 = -0.05°$ or for $\gamma = -0.05°$, with $\delta_1 = \delta_2 = +0.05°$.

When the diffractometer is nearly, but not yet fully, aligned, the tilts δ_1 and δ_2 are both finite but small (of the order of $\pm 0.1°$). However, as long as both these tilts are non-zero, the 'best' instrumental alignment is through an interplay among all three misalignment parameters listed earlier. In such cases, the sharpest diffraction peaks occur approximately when δ_1 and δ_2 have similar values but opposite signs (Fig. 3). On the other hand, in the well aligned instrument, only the second crystal tilt δ_2 has to be adjusted. In this case, the maximum alignment occurs under condition of minimum tilt δ_2 (Fatemi, 1989, 1996). In general, therefore, one needs to examine the relationship among the various misalignment factors in some detail.

Table 2 lists, for the purpose of illustration only, the numerical results θ_c for several combinations of the three parameters γ, δ_1 and δ_2, each having values of $\pm 0.05°$ (~3 arc min), using Si 004 and Si 224 reflections. The algebraic difference between the shift errors or 'residue' is also given in the last two columns for the '3 arc min' and the '1 arc min' cases, respectively. We see that for each set of parameters the shift errors for the two reflections have similar signs and magnitude. Their difference in each case results in a number significantly smaller than each shift error individually. It is clear that both θ_1 and θ_2 in the original equations (1a)–(1d) are affected by two unknown errors of similar magnitude.

The difference $\theta_{2c} - \theta_{1c}$ is thus the only significant quantity in the calculation of misalignment errors. The expression for this residue is given by

$$\theta_{c2} - \theta_{c1} = -\frac{\delta_2^2 + \Psi^2}{2}(\tan\theta_2 - \tan\theta_1) + \Psi\delta_2\left(\frac{1}{\cos\theta_2} - \frac{1}{\cos\theta_1}\right),$$

(27)

which in the case of an Si (100) wafer with 004 and 224 reflections and Cu $K\alpha_1$ becomes

$$\theta_{c2} - \theta_{c1} = -0.227\frac{\delta_2^2 + \Psi^2}{2} + 0.176\Psi\delta_2.$$

(28)

The part of the error shared by θ_{1c} and θ_{2c} is effectively a fixed unknown adjustment that is removed by the zero-offset calculation. Thus, the residue shows the disparity between the reflections due to misalignment. In Table 2, we also see that reducing δ_1, δ_2 and γ from 0.05° (3 arc min) to 0.02° (~1 arc min) reduces the shift errors by nearly sixfold. These numbers are also obtained within the round-off errors from equation (28). Note that a 0.02° deviation from the horizontal is equivalent to a vertical shift of $\approx$7 mm in 20 m. Hence, a laser level can be used to align the pinhole collimator with relative ease within this tolerance.

4.2. A numerical estimate of the shift error

While the residual error e could be taken as an uncertainty in one of the two angular measurements, its eventual effect is on the zero offset ε, which changes both θ_1 and θ_2. To examine the effect on θ_c, we assume that e arises mainly from the second measurement θ_2. One could show, however, that the analysis would not be affected if the residue were shared between both measurements. The true offset ε_e can then be expressed as

$$\varepsilon_e = \frac{\alpha\sin(\theta_2 + e) - \sin\theta_1}{\cos\theta_1 - \alpha\cos(\theta_2 + e)} \cong \varepsilon + \frac{\sin\theta_1}{\tan\theta_2}e,$$

(29)

where the residue $e \ll \theta$, and ε is the value defined in (6). We see that the zero offset is altered by an amount of the same order as e. Calculating the effect of this adjustment in ε on the measured angles θ_1 or θ_2 (004 or 224, respectively), we get

$$\delta\theta_i = \delta\varepsilon\cos^2\theta_i,$$

(30)

where $\delta\varepsilon$ is defined by the second expression in equation (23). In the present example, the shift in the measured angle is about $0.4e$. Ignoring the least likely results in the last row of Table 2, this is of the order of $0.8 \times 10^{-5\circ}$ for the '3 arc min' deviations, and $1.5 \times 10^{-6\circ}$ for the '1 arc min' case, both numbers well outside the digital capabilities on most diffractometers. The corresponding effects on Si 004 reflection would be $\pm 1.1 \times 10^{-6}$ and $\pm 2 \times 10^{-7}$ Å, respectively. The one order-of-magnitude difference here is purely academic, as most applications do not require this level of precision. The ideal instrumental accuracy in the method may therefore be taken, conservatively, as the larger number, 1×10^{-6} Å, which for Si is equivalent to nearly 2 parts in 10^7.

The practical precision in the method, however, depends on a number of factors including the quality of the crystal being examined, the choices of various reflections used in the measurements, and the extent of mechanical and thermal instabilities in the system. The most important among these are warping and mosaicity. The zone technique emphasizes the use of small sample area and limiting the measurements to higher Bragg angles. This practice reduces the effects of inhomogeneity and warping, but does not by itself eliminate the uncertainties caused by changes in the penetration depth caused by mosaicity as a function of angle and wavelength, especially if only a few rocking curves are used. Similar problems are of course encountered in the comparative technique. In order to analyze lattice-parameter variations with depth or thickness, more elaborate measurements with various wavelengths and incidence angles would be needed. For most materials of interest in the electronics area, however, the effect is found to be negligible, and in the author's past experience different zones and reflections in a single system have yielded nearly identical results, subject to the following caveat.

The choice of the particular diffracting planes does raise questions about the consistency of the results, since the measurements may not always correspond to the same area of the sample, nor to the same depth of penetration (Fewster, 1985). Similarly, the assumption of a particular symmetry does not always hold, as for example in the case of electronic grade Si, which is expected to be fully cubic. This can often be seen in routine measurements of the 111-type reflections in Si, in which the 222 reflection is forbidden, but is nevertheless observed, at times with significant intensity. This suggests that the specific crystal structure chosen in the zone technique should be at least partially verified by comparing the lattice parameters obtained from various combinations of reflections.

4.3. Eccentricity effects in the Bond and the zone techniques

Eccentricity plays an important part in characterizing crystals of intermediate perfection, particularly when warping is present. It can occur for any combination of offsets between the ω axis, the X-ray beam and the crystal surface. Its contribution, no matter how small it seems, should therefore be verified accurately. While the probability for physical offsets is small for factory-aligned instruments, caution is nevertheless warranted. It is thus worthwhile to compare the effect for the zone and the Bond methods. Here we consider only the displacement between the ω axis and the crystal surface, the distance labeled h in Fig. 6. We assume that the crystal surface is polished flat, and that it has been aligned initially parallel to the incident beam by reducing the beam intensity by one-half. This customary practice has often been misinterpreted as the *main* requirement to 'center' the crystal in the beam, whereas in fact it merely aids in establishing an approximate starting point for the measurements.

In Fig. 6, the three orientations of the wafer denoted by [0], [I] and [II] correspond to the 'starting point', the $(n, -n)$, and the $(n, +n)$ settings, respectively. Point O marks the base of the

perpendicular from the ω axis to the sample surface. In the Bond technique, the crystal would be turned by the angle between positions [I] and [II]. During this rotation, the crystal surface remains tangent to the circle of radius h and the beam strikes the sample at points A and B in orientations [I] and [II], respectively. In the absence of eccentricity ($h = 0$), the beam would be diffracted from the same point on the crystal surface, whereas, for $h \neq 0$, the distance AB has no effect on the measurements for atomically flat planes. For curved planes, however, the actual angle between the two peaks would no longer be $\pi - 2\theta_B$. The discrepancy would depend on the dimension h, the incidence angle θ and the curvature of the diffracting planes. Ignoring any second-order effects of displacement due to warping, the distance AB can be written as

$$AB = OB - OA \approx \frac{h}{\sin(\theta/2)} - h\sin(\theta/2). \quad (31)$$

To estimate this distance, we assume the single-crystal wafer to be a (100)-oriented Si wafer, with θ_B (004) $\approx 34.564°$ using Cu $K\alpha_1$ radiation. Let $h \cong 0.2$ mm, comparable to the apparent width of a typical X-ray focal spot or, similarly, the thickness of a typical single-crystal wafer. This yields AB $\cong 3h = 0.6$ mm. We also assume that, while the surface is flat, the (001) planes are curved to a 'large' radius $R_c = 10$ m, concave toward the rotation axis. At peak diffraction, the angle between the incident beam and the (001) planes at point B would therefore be larger than that recorded on the ω scale by the amount

$$\Delta\theta_e = AB/R_c. \quad (32)$$

In the present case, $\Delta\theta_e \simeq 6 \times 10^{-5}$ rad $= 0.0034° = 12.4$ arc s. This means that in order to reach the peak diffraction in the ($n, +n$) mode the wafer would have to be placed at a smaller
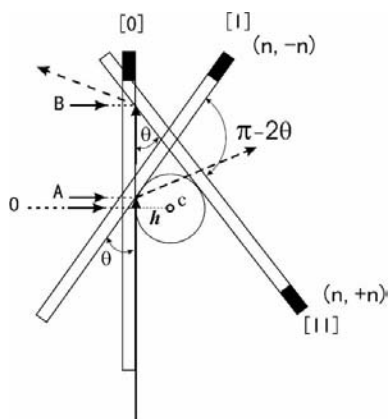
Figure 6
Eccentricity effects in the Bond and the zone techniques. Orientations marked by [0], [I] and [II] in the Bond method correspond to the starting point, the ($n, -n$) and the ($n, +n$) configurations, respectively. The ω axis passes through the center of the small circle whose radius h is the 'eccentricity' between the ω axis and the crystal surface. During the measurements, the crystal surface remains tangent to this circle, such that in positions [I] and [II] the beam strikes the surface at points A and B, respectively. The dimension h and the distance AB affect the measurements in warped or curved crystals, but not in atomically flat crystals. In contrast, the narrower range of angles in the zone technique produces a much smaller error of eccentricity.

angle, leading in turn to a larger separation of $\pi - 2\theta_B + \Delta\theta_e$. The 'interpreted' value of θ_B for the 004 reflection would then be too small by 6.2 arc s, corresponding to an error in the calculated lattice parameter of about 0.00023 Å.

In the zone technique, by contrast, only the shifts in point A are involved, as the ($n, +n$) reflections are not used. The maximum angular 'error' occurs between the two asymmetric 224 reflections ($\omega_{shl} = 8.75°$, $\omega_{stp} = 79.2°$):

$$\Delta l = h[\sin(\omega_{st}/2) - \sin(\omega_{sh}/2)] = 0.11 \text{ mm.} \quad (33)$$

Using the same numbers as before, the corresponding change $\Delta\theta_e$ due to curvature is now 1.1×10^{-5} rad or 2.26 arc s. Again, since the Bragg angle is obtained from the average of two measurements, the maximum error in this case (224 reflection) is 1.13 arc s. This is nearly one-sixth the corresponding error in the Bond technique.

It is clear that for high-precision measurements the beam must be centered as precisely as possible on the rotation axis. To perform this alignment, a vertical slit of desired opening is placed at the sample position and an incident X-ray beam of similar width is made to pass through the slit, first at $\omega = 0°$, then at $\omega = 180°$ positions. The beam is considered centered if the same intensity is recorded at both settings without the need for adjustments. Otherwise, both the sample holder and the beam conditioner are readjusted until the proper alignment is reached.

4.4. Comparison of the zone and the triple-axis techniques

Recently, Fewster & Andrew (1995) introduced a novel procedure for absolute lattice-parameter measurements on a triple-axis diffractometer. The method was a significant improvement over the Bond technique, as it allowed full characterization of thin films and their substrates. In that method, each diffracting plane is separately aligned parallel to the ω axis, and the detector zero setting is also separately adjusted for each particular $2\theta_B$. For a crystal initially oriented at random, the same diffraction peak can be reached in various ways. The diffracting plane can often be aligned by adjusting the tilt alone, by the crystal azimuth alone, or yet again by any suitable combination of the two movements. For each reflection, therefore, the 'true' $2\theta_B$ angle is reached with a separate zero correction. The main advantage of the triple-axis method lies with the less perfect mosaic crystals of constant composition (uniform d spacing), which with proper beam conditioning can produce extremely sharp ω–2θ diffraction peaks, whereas in the zone technique such materials yield rocking curves whose width (FWHM) is sensitive to the degree of mosaicity and crystalline quality.

Although the general procedure for sample alignment in the two types of instruments is nearly the same, there exist a few distinguishing aspects.

A major difference is in the detector window size. In many triple-axis measurements, the detector window is vertically extended to capture most of the diffracted intensity from large sample areas. However, the detector reading can be influenced by misalignments in both tilt and azimuth, since these would

redirect the beam to a spot other than the center line. This change in the beam position could be easily overlooked, since the detector response is nearly constant in an extended vertical direction. Yet, as analyzed in a similar fashion elsewhere (Fewster & Andrew, 1988), the actual detector reading will probably not correspond to the correct $2\theta_B$. Fig. 7 shows an exaggerated graphical representation of this effect.

Assume that the incident and diffracted beams are contained in an inclined plane where the angle between them is $2\theta_B$. The angle measured at the detector position is $2\theta_m$, the vertical 'projection' of the angle $2\theta_B$ onto the horizontal plane. Depending on the relative orientation of the incident and diffracted beams, this angle may be smaller than $2\theta_B$ (Fig. 7a), larger than $2\theta_B$ (Fig. 7b), or seldom also equal to it (not shown). It is clear that these errors are less likely to occur the smaller the vertical opening in the detector widow. The shorter window thus increases the sensitivity of sample alignment to deviations from the correct tilt and azimuth.

Another difference between the two techniques concerns the angles used in the measurements and their ultimate resolution. The double-crystal technique employs an ω scale with a typical step size of $0.0001°$, but does not require extremely precise placement for the detector itself. In contrast, the detector angle in the ω–2θ geometry can be set to a step resolution of twice that number for equal precision.

Finally, eccentricity, which is non-existent for flat crystals in the double-crystal diffractometer, often remains an issue in some ω–2θ techniques especially those requiring measurements from several planes; unless, of course, the beam is properly aligned and probes only a fixed well centered sample area. The eccentricity problem also remains in the case of

Figure 7
The angle measured through a detector with a vertically extended window may be influenced by the inclination of the incident and diffracted beams with respect to the diffractometer table. This angle would only equal $2\theta_B$ if the beam segments from the X-ray source to the detector were in the plane of the diffractometer. The measured angle may be larger or smaller than $2\theta_B$ as shown in (a) or (b).

triple-crystal diffractometers employing $(m, +m, \pm n)$ geometry using the Bond technique in the double-crystal mode, despite the fact that the reflection angles *per se* can be accurately determined with the aid of good intensities and high resolution using four-crystal monochromators (Bartels, 1983).
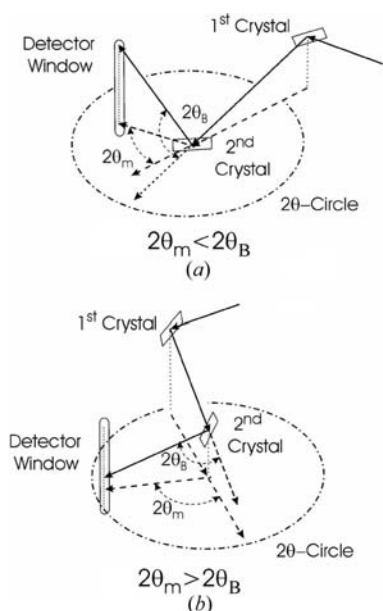
5. Discussion and conclusions

In this paper, the practical advantages and features of the zone technique were highlighted and discussed in detail. It was shown that lattice parameters and strains in single-crystal layers can be measured easily and rapidly on a double-crystal diffractometer with only a few rocking curves. The concept of strain in typical structures was examined. Consistent with the familiar expression for the strain in the cubic crystals, a slightly different formulation was introduced for the hexagonal crystals. The practical errors of measurement caused by misalignments were calculated for the zone technique, and an ideal detection limit of better than ± 2 parts in 10^7 was established for nearly perfect layers. The process credited for this high accuracy is intrinsic to the zero-offset calculation. This number of course does not take into account such factors as the mechanical stability in the system, reproducibility of the angle settings, sample non-uniformities and temperature fluctuations.

We note that the use of the zone technique does not vitiate the need for the comparative approach, which can indeed be utilized in several helpful ways. One example is in the measurement of the interlayer tilt, which is handled quite rapidly by the comparative technique. Knowledge of this angle helps to simplify the absolute measurement of tilted layers further, since it allows one to choose the sample orientation such that the tilt is either minimized or eliminated altogether.

Combining the two techniques is also helpful for very thin epitaxic films by taking advantage of higher diffracted intensities at lower angles. The low-angle data are not usually deemed suitable for the zone technique: not only are their refraction corrections less accurate, but also the wider area of the sample covered by the beam contributes to errors due to surface inhomogeneities. Nevertheless, one can at times obtain satisfactory results with such data: when both layers are measured at similar angles, they are subject to similar beam profiles or 'footprints'. The relative peak separations measured in the comparative method are also far less sensitive to instrumental misalignment than each peak in the pair measured alone.

This would suggest an 'indirect' way of characterizing thin epilayers relative to the substrate, which is first characterized absolutely with a high-order symmetric and two asymmetric reflections. Assuming that the 002 reflection is allowed, a rocking curve is then recorded for both the epilayer and the substrate in the comparative mode. The two peaks are then corrected for their interlayer tilt, if any, and for the zero offset calculated from the high-angle data. Finally, the 'absolute' 002 peak is computed for the epilayer by reference to the substrate, to yield its corresponding lattice parameter.

Among interesting applications of the zone technique presently under study are the measurement of GaAlAs layers grown on GaAs aimed at establishing the precise calibration constant for Al concentration, the measurements of non-polar GaN layers on *r*-plane sapphire, and the tilt and rotation effects in wafer bonded structures.

References

Baker, T. W. George, J. D. Bellamy, B. A. & Causer, R. (1966). *Nature (London)*, **210**, 720–721.

Bartels, W. J. (1983). *J. Vac. Sci. Technol.* B**1**, 338–345.

Bond, W. L. (1960). *Acta Cryst.* **13**, 814–818.

Cullity, B. D. (1987). *Elements of X-ray Diffraction*, 2nd ed. Reading, MA: Addison-Wesley,.

Dismukes, J. P., Ekstrom, L. & Paff, R. J. (1964). *J. Phys Chem.* **68**, 3021–3027.

Fatemi, M. (1989). *J. Cryst. Growth*, **96**, 316–326.

Fatemi, M. (1990). *Advances in X-ray Analysis*, Vol. 33, edited by C. S. Barrett, J. V. Gilfrich, T. C. Huang, R. Jenkins & P. Predecki. New York: Plenum Press. Proceedings 38th Ann. Conf. on Applications of X-ray Analysis, Denver, CO, USA, p. 83.

Fatemi, M. (1996). *J. Cryst. Growth*, **169**, 261–268.

Fatemi, M. (2002). *Appl. Phys. Lett.* **80**, 935–937.

Fatemi, M. & Stahlbush, R. E. (1991). *Appl. Phys. Lett.* **58**, 825–527.

Fatemi, M., Stahlbush, R. E., Twigg, M. E. & Neudeck, P. G. (2004). Unpublished.

Fewster, P. F. (1985). *J Appl. Cryst.* **18**, 334–338.

Fewster, P. F. & Andrew, N. L. (1988). *Thin Solid Films*, **319**, 1–8.

Fewster, P. F. & Andrew, N. L. (1995). *J Appl. Cryst.* **28**, 451–458.

Fewster, P. F. & Curling, C. J. (1987). *J. Appl. Phys.* **62**, 4154–4158.

Gałdecka, E. (1999). *International Tables for Crystallography*, Vol. C, 2nd ed., edited by A. J. C. Wilson & E. Prince, pp. 501–531. Dordrecht: Kluwer Academic Publishers.

Hart, M. (1969). *Proc. R. Soc. London Ser. A*, **309**, 281–296.

James, R. W. (1963). *Solid State Physics*, edited by F. Seitz, pp. 118–121. New York: Academic Press.

Kikuta, S., Kohra, K. & Sugita, Y. (1966). *Jpn. J. Appl. Phys.* **5**, 1047–1056.

Lee, W. E. & Lagerloff, K. P. D. (1985). *J. Electron Microsc. Tech.* **2**, 247–258.

Maslen, E. N., Fox, A. G. & O'Keefe, M. A. (1999). *International Tables for Crystallography*, Vol. C, 2nd ed., edited by A. J. C. Wilson & E. Prince, pp. 548–584 Dordrecht: Kluwer Academic Publishers..

Thomsen, J. S. (1973). *X-ray Spectroscopy*, edited by L. Azároff, pp. 57–80. New York: McGraw-Hill.

Wie, C. R. (1989). *J. Appl. Phys.* **66**, 985–988.

Zhang, X., Sugiyama, H., Ando, M., Imai, Y. & Yoda, Y. (2003) *J. Appl. Cryst.* **36**, 188–192.